

ANALYSIS OF SUCKER ROD AND SINKERBAR FAILURES

by
John R. Waggoner
Advanced Technology Department
and
Rudy G. Buchheit
Mechanical and Corrosion Metallurgy Department

Sandia National Laboratories
Albuquerque, NM 87185

Abstract

This paper presents results from a study to analyze the performance and failures of the sucker rod/sinkerbar string used in beam-pumping operations through metallography, structural finite element analysis, and detailed failure data collection. Metallography has demonstrated that the microstructure of the steel bar stock needs to be considered to improve the fatigue resistance of the sucker rod strings. The current specification based on tensile strength, or yield strength, may not be appropriate since failure occurs because of fatigue and not yielding, and tensile strength is not always a good measure of fatigue resistance. Finite element analysis of the threaded connection identifies stress and fatigue concentrations and quantitatively assesses the performance and failure of coupling designs under a variety of loading conditions. Subcritical fractures observed in the metallography are also suggested by the calculated stress distribution in the threaded coupling. Failure data illustrates both the magnitude and frequency of the failures, as well as categorizing the suspected cause of failure. This detailed failure information alone can reduce failures by indicating specific problem areas where focused action can yield immediate results.

Application of the results in each of these project areas is expected to yield improved choice of metal bar stock, thread design, and make-up practices which can significantly reduce the frequency of sucker rod failures. Sucker rod failures at the rates observed today are not inherent in the process, but can be minimized through the application of new technology and observation of common-sense practices.

* Work performed at Sandia National Laboratories under DOE contract DE-AC04-76DP00789.

Introduction

In 1977, 92.7% ¹ of all US oil producing wells were being artificially lifted, i.e. oil production was assisted by operator intervention. Of these artificially lifted wells, 85.2% were rod-pumped, meaning that the surface generated pumping motion is transmitted to a downhole pump via a string of rods. If we assume that these percentages remain the same as the number of US oil producing wells has increased from 518,867 in 1977 ¹ to 597,320 in 1990 ², there were about 472,000 rod-pumped wells in the US in 1990.

While the frequency of failures in these rod-pumped wells varies greatly from field to field, it is not uncommon for 2/3 of these wells to experience a downhole failure each year, resulting in 2-3 days of no production and \$2500 for each workover. On a national scale, this amounts to \$780 million spent annually on rod-pumped well failures, not including the value of the oil production delay. In addition, about 85% of the rod-pumped wells are stripper wells producing less than 10 b/d oil. For these wells, continued operation depends strongly on projected maintenance costs. A large part of the US petroleum resource, therefore, is directly influenced by the frequency of failures in rod-pumped wells.

This paper describes a scoping study at Sandia National Laboratories (Sandia) to analyze the failure of sucker rod and sinkerbar coupling failures. Following a discussion of the background and objectives of the project, each of the three major research areas - failure data collection, finite element analysis of the coupling, and metallographic analysis of failed couplings - will be described with associated results.

Background and Objective

Successful and profitable operation of secondary recovery oil wells is compromised by downhole equipment failure. A major component of downhole equipment is the sucker rod string which connects the pump jack on the surface with the pump at the base of the well. Well depths may reach 10,000 feet or more ³. Sucker rod strings are generally comprised of 25 foot long "rods" connected by "boxes" or couplings. Typically, rods have threaded male ends that fit into the female boxes. Rods and boxes are made from steels and are furnished to operators according to an API specification described below. Should a string break, production ceases since well pressure is insufficient to force crude-bearing fluid to the surface. A repair operation ensues: the top portion of the broken string is withdrawn, while the bottom half is extracted by a "fishing" procedure.

Operation of secondary recovery wells without downhole equipment failure is highly desired, but difficult to achieve. According to an article from Petroleum Engineer International an amazing set of precautions must be taken to obtain reliable downhole equipment performance ⁴:

A sucker rod string properly designed based on practice and experience, physically handled in accordance with recommendations of manufacturers, run using correct makeup and breakout procedure, properly operated, and with effective downhole corrosion control should give a long, satisfactory, and economical service life.

In fact, field data show that when these precautions are taken, failure incidence is significantly reduced. Rigorous maintenance programs for downhole equipment with emphasis on following the prescribed string breakout and makeup procedure have a strong positive impact on service life ⁵. Computer-aided design of strings has also had a beneficial effect reducing failures. On the negative side, downhole corrosion control has traditionally been

complicated by economics, logistics and the uncertainties associated with determining the effectiveness of corrosion control techniques ^{6,7}.

A recent adaptation of sinker bar pin designs for sucker rods appears to have a beneficial effect on string performance ⁸. Sandia was asked to further characterize the performance benefit associated with the adapted pin design, and so, on January 31, 1992, Mr. Don Bennett, President of Flexbar, Inc., arranged and hosted a meeting of industry personnel in Midland, TX to discuss current problems with sucker rods/sinker bars in oil production ³. Through discussions at this meeting and with others from industry, it became apparent that this was an area where DOE support through the Oil Recovery Technology Partnership would give widespread help to the petroleum industry. Between February and May, 1992, Sandia National Laboratories (Sandia) has performed a scoping study consisting of metallographic examination of failed sucker rod pins, a finite element analysis of the threaded connection, and gathering data and experience about sucker rod failures by collection of rod pumped well failure reports from industry. The overall objective of Sandia's program is to reduce the rate of rod-pumped well failures and thus improve the economics of production operations through the application of high technology tools developed and/or used at the labs.

Data Collection

Prior to about 1986, most oil well operators discarded a failed pin or coupling, and many continue to do so today. Since then, however, some operators have been collecting the failures, or at least collecting data on the type, location, and probable cause of every failure. This data collection effort has created a database that describes the severity of the sucker rod failure problem and hints at what should be done to alleviate the problem. Collection and analysis of this data has allowed the operators to reduce the problem by improving field practices, but even with this significant effort, the problem will not go away. It is apparent that the 1950's technology in use today, even with the best field practices, are not sufficient to solve the problem, and the application of 1990's technology is warranted.

Throughout this project, many people in the petroleum industry have related their thoughts and experience with the rod pumped well failure problem. While the initial focus was on the performance of the threaded rod connection, it became apparent that failures in the tubing and downhole pump are at least as troublesome as the rod string failures. In addition, all agreed that the rod pumped well failure problem was widespread, costly, and the result of using 1950's technology without significant improvement.

To quantify the failure problem, failure data from industry personnel located in the Midland area was obtained and analyzed. The data covers more than 3000 wells from 1986 to 1991, including detailed failure analysis from one field over a 6 month period in 1992. Both datasets have been extremely useful in documenting the magnitude of the failure problem.

The following observations can be summarized from the data:

- By keeping failure analysis records and taking corrective actions, the frequency of failure has declined. Improved field practices do help, but the problem is still significant.
- Failure frequency (FF), the number of failures per well per year, varies from field to field, but numbers near and above 1 are not uncommon.

- When divided into 3 categories (i.e., rod string, tubing or pump failures), pump failures are the greatest in number, followed closely by rod string failures, and then tubing failures. However, approximately 25% of pump failures are due to particulates seizing the pump or sticking the valves, and so are not actually mechanical failures. This makes rod string failures the most common downhole mechanical failure.
- The 3 categories of rod string failures are interrelated through the dynamic performance of the entire rod pumping system.
- There may be a correlation between rod and tubing failures, although adequate data is not available to prove this. If a rod string buckles, most commonly in the 3/4" rods, the rod connection is subjected to an applied bending moment, and the tubing is subjected to increased friction and banging forces. This banging can also cause a rod connection to unscrew, resulting in failure.
- Buckling in the rod string can result from downhole pump operations which were not modeled by the design code. Specifically, increased friction will increase both the tensile and compressive loads on the string, and fluid pound can cause the pump piston to bang against the bottom seat of the pump and increase the vibration in the string.
- At a FF of 1 in a field of 116 wells, there are 116 failures per year. For an average workover time of 3 days at a cost of \$2500, this amounts to 348 days of lost production, and \$290,000 spent. The economic impact of this FF depends on the productivity of the well and the price of crude oil, but it is sure to be a significant cost even for the major oil companies.
- There are approximately 400,000 stripper wells in the US, most of which are rod pumped. At a FF of 1 for these 400,000 wells, \$ 1 billion is spent annually on well failures. Given that stripper wells are often marginally economic, the cost of a well workover may lead to premature abandonment of some wells and loss of resource.
- Chemical corrosion is a significantly large cause of failure in rod strings. Even when corrosion inhibitors are used in the well, the friction between rods and tubing remove the inhibitor layer and expose the steel to corrosive fluids. Since all wells are deviated to some degree, resulting in the rods riding on the low side of the casing, it is likely that many wells will be subjected to this class of failure.

Finite Element Analysis

During this scoping study, Sandia has developed and demonstrated a finite element analysis of the threaded sucker rod connection. Finite element analysis is a relatively inexpensive method (compared to experimental) to quantitatively assess characteristics of a given connection design and to compare differences between alternative designs. In addition, the analysis can be conducted at a variety of loading and prestress conditions. This paper summarizes the approach, mesh generation, and finite element simulation needed to develop

this threaded coupling simulation capability, and then demonstrates the capability with sample results.

Approach

A detailed 2-D axisymmetric representation of the threaded connection is used for this static analysis of the threaded connection. It is beyond the scope of this report to simulate the dynamics of the connection, which would require a 3-D representation. For demonstration purposes, a 7/8" API sucker rod box and pin connection was chosen for this analysis. The API specifications on the dimensions of the connection (API SPEC 11B) ⁹ were followed exactly when possible. When a range of acceptable values was specified, the value resulting in the minimum thread contact was chosen as a worst case scenario. Figures 1 and 2 illustrate both the dimensions used in this analysis and the terminology used in this report. A pre-processing program allows for rapid generation of standard API box and pin connection sizes.

Mesh generation

The mesh is generated by FASTQ ¹⁰, Sandia's finite element mesh generation program, using the paving algorithm. The mesh used in this study consists of 3497 nodes and 3329 elements. This level of refinement reasonably represents the geometric complexity while keeping the mesh size small enough to allow rapid analysis during this scoping phase. However, it may not be fine enough to capture very localized high stress features. Further mesh refinement for subsequent analysis should eliminate most of the warnings of distorted elements and increase the accuracy of the analysis.

ABAQUS simulation

The finite element code used in this study is ABAQUS ¹¹, which is well suited to this type of analysis and can be extended if more complex analysis is desired. Four node bilinear axisymmetric solid elements used for the box and pin bodies and 2 node slide line elements are defined to model the contact surfaces along the threads and shoulder.

Prestress in the connection is achieved by lengthening the box to overlap the pin at the shoulder. Since two solid parts cannot occupy the same space at the same time, the overlap is non-physical and is resolved automatically by the finite element simulator by lengthening the body of the pin, thus creating the desired tensile prestress. The amount of overlap depends on the desired prestress in the pin and the physical dimensions of both the box and pin according to the following procedure. The desired tensile prestress in the pin is divided by the Young's Modulus of the steel to calculate the needed strain in the pin. This elongation must be accompanied by a compressive strain in the box due to the force transmitted through the thread. Since the cross-sectional areas of the pin and box are not equal, the compressive stress in the box is not the same as the tensile stress in the pin, and thus the strain in the box will not be the same as the strain in the pin. As defined by the API specification, the thread faces are not initially in contact. The gap between thread faces that will come in contact is calculated, and added to the tensile strain in the pin and compressive strain in the box to arrive at an estimate of the overlap needed to achieve the desired pin prestress. With the current mesh size, establishing the prestress condition take about 700 CPU seconds on a CRAY-XMP.

Analysis of loading conditions on the connection is achieved by applying an axial load on the distant end of the box. A tensile load will represent the effective weight of the fluid immersed rods below this connection plus the weight of fluid, inertial effects, and friction. A compressive load will represent a condition which should only occur at the bottom of the rod string, if at all. Compressive forces are avoided because of the tendency of long, thin strings to buckle in compression. This model will not predict buckling behavior.

The von Mises effective stress is used to identify areas that are susceptible to failure. A failure criteria based on the von Mises stress can be used to locate points of expected failure, but the actual failure cannot be modeled. For this study, identifying the location and magnitude of large von Mises stress is sufficient to analyze and compare alternative designs. The current analysis uses a simple purely elastic constitutive material model for the box and pin bodies. ABAQUS will easily handle the elastic plastic behavior of the metal once it is defined.

Sample Results

A 7/8" API sucker rod box and pin connection was simulated using the procedure described above. The dimensions of the joint are shown in Figures 1 and 2. The Young's Modulus (30.5E6 psi) and Poisson's Ratio (0.3) are typical for the steels used in sucker rods, but no plastic behavior data was used. The shoulder overlap (0.006 in.) was calculated for a desired prestress of 40,000 psi (tension) and thread gap of 0.0046 in.

Figures 3, 4 and 5 consist of a set of 4 figures labeled 'a' through 'd'. The 'a' figure shows the entire joint to give an overall perspective of the figure. Figure 'b' zooms in to show the first four engaged threads in some detail, and figure 'c' zooms in further to show the first engaged thread and the initial partial thread on the box. This view is critical in that field samples indicate that failure most commonly occurs at the base of the first engaged thread. Figure 'd' shows the shoulder contact region at the same level of zoom as figure 'c'. This view is also very important because failure has been observed at the start of the undercut region and this is the region modified by one of the prospective designs to be evaluated in a later study.

Figures 3a-d show the undeformed mesh used in the simulation. Figure 3a illustrates the density of elements around the threads compared to the body of the pin and box. The rapid transition from fine to coarse gridding produces the distorted elements that result in ABAQUS warnings. A finer mesh away from the threaded region will alleviate this problem. Figure 3b details the first four threads as initially defined to be separated, and more clearly shows the rapid change in element density. Figure 3c shows the thread mesh even more clearly, and also shows the thread gap (axial distance between matching nodes along thread contact surface) that will be used in the calculation of the shoulder overlap, shown in Fig. 3d.

Figure set 4 shows contours of the axial stress component. Negative values of axial stress represent compression while positive values represent tension. The zero value of axial stress falls between contour lines D and E. The maximum value of tension, marked by the asterisk in Figs. 4a and 4d at the base of the undercut, is 31,000 psi, not the 40,000 psi prestress desired. In fact, the stress in the undercut region of the pin is less than 25,000 psi. This leads to an ambiguity in what the desired prestress value means since stress varies across the pin. This issue is beyond the scope of this study. The maximum value of compression is over 62,000 psi, marked by the circled cross in Figs. 4b and 4c at the root of the first box thread. This is clearly a critical area since it carries considerably more stress than the thread contact and shoulder (15,000 to 35,000 psi) which are generally considered to carry the most compressive load. These values can be compared with the yield strength of the material to indicate when yielding will occur, but an elastic plastic constitutive model is also needed to model the effect of plastic deformation.

Figure 4b also shows a line labeled E extending from the contact face of each thread to the root of the next thread in the pin. A zero contour would lie close to E and on the thread side of E. This is a region of transition from compression at the contacted thread face to tension in the body of the pin, and coincides well with the position of micro fractures observed in metallography studies of failed sucker rod pins (see Figure 10). Further research is needed to identify the relationship between these two observations. Also note that the first engaged thread is the only one in the pin to show the D contour level, indicating that this single thread is

carrying the majority of the load. This observation is consistent with general knowledge of threaded connection behavior.

Figure set 5 shows contours of von Mises effective stress. All values are positive with larger values indicating a tendency to fail. A von Mises failure criteria was not calculated in this analysis. The minimum value is located at the last engaged thread shown in Fig. 5a, clearly an area which is unlikely to fail. The maximum value of over 63,000 psi is again located in the root of the first box thread, emphasizing the possibility of failure at this point. The next largest contour level observed is C, located at the root of the first engaged thread in the box, and the two curvatures in the undercut region of the pin. Only after calculation of the von Mises failure criteria, however, will these von Mises contours become useful analysis tools for comparing the relative performance of different joint designs.

Metallurgy

The API Specification for Sucker Rods

The chemical and mechanical properties of steels that may be furnished under the American Petroleum Institute (API) Specification for Sucker Rods (Pony Rods, Polished Rods, Couplings and Subcouplings)⁹ is quite broad. The breadth of acceptable steel compositions is necessary given the wide range of operating conditions that are encountered in secondary recovery wells. The API specification for sucker rods calls out three specific grades of sucker rods that are distinguished primarily by their ultimate tensile strength. In general, any plain-carbon or alloy steel that can be heat treated to the minimum ultimate tensile strength for that particular grade, is considered to be furnished in accordance with the specification. However, 46xx (low carbon 0.10 to 0.25 weight pct., 0.85 to 1.83 Ni, 0.20 to 0.25 Mo) and 15xx (medium carbon 0.25 to 0.55, 1.35-1.65 Mn) are specifically called out.

In general, alloys steel provide a number of advantages over plain-carbon steels. When considering the use of plain-carbon steels in sucker rod strings, the following limitations must be recognized:

- 1) Plain-carbon steels cannot be strengthened beyond 100 ksi without a ductility and toughness penalty.
- 2) Rapid quench rates are necessary for full hardening of medium carbon plain-carbon steel. Rapid quenching often results in shape distortion and cracking.
- 3) Plain-carbon steels typically have lower corrosion resistance than alloy steels.

Although alloy steels may be more expensive, their use may be more economical in the long run.

Microstructural Characterization of Field Return Specimens

A random sample of 15 failed sucker rod pins and coupling boxes returned from service were provided to Sandia by Exxon Production Operations/Southwestern Division¹². Additional pin samples that had not seen service were provided to Sandia by Flexbar, Inc. These samples were examined for comparison to the field returns. Pins and boxes were sectioned, wet polished and etched to reveal microstructural elements present. Optical microscopy was used to qualitatively evaluate microstructure and check for the presence of cracks.

Optical microscopy showed that each of the pins and boxes examined exhibited ferrite-pearlite microstructures commonly observed in low to medium carbon plain-carbon and alloy

steels allowed in the API specification. The wide variations in the appearances of these microstructures are due to the use of different steel compositions, differing prior austenite grain sizes and processing histories. For steels called out in the API specification, desired mechanical properties can be achieved by normalizing, or quench and tempering. Hot rolled rod stock provided in the as-received condition may also provide adequate mechanical properties. Described below are three distinctly different microstructures that were observed in the specimens examined.

Figures 6a and b are optical micrographs of pin samples from the lower grade sucker rod provided by Flexbar, Inc. In these micrographs, the large dark areas are comprised of pearlite, which is actually alternating cementite (Fe_3C) and ferrite (an Fe-C solid solution) lamellae, and light areas of proeutectoid ferrite. The ferrite grains appear to reside on prior austenite grain boundaries giving the "network-like" appearance at lower magnification. This microstructure is observed in medium carbon plain-carbon steels and in manganese steels (like 15xx) when these steels are normalized by austenitizing. During austenitizing the steel is transformed to stable austenite. The steel is then cooled (quenched) and the austenite transforms to proeutectoid ferrite and pearlite. The relative proportions and distribution of ferrite and pearlite depend on a variety of factors but are predominantly influenced by carbon content, cooling rate, and prior austenite grain size. This distribution of ferrite and pearlite in Figure 6a and b is consistent with an air quench. The effects of tempering on microstructure are typically too slight to distinguish by optical microscopy.

Figure 7a and b are micrographs from pins taken from Flexbar's higher grade sucker rod. Here, the light phase takes on a plate-like morphology consistent with Widmanstätten ferrite. The dark regions appear to be pearlite but, individual lamellae can not be resolved. Microstructures of this type can be produced in two ways. In plain-carbon steels fine pearlitic structures can be formed if quenching is rapid enough. However, since the rod stock used to for sucker rods is 1 inch or greater in diameter, the quench rate may not be sufficiently fast at the center of the rod to generate a homogeneous microstructure throughout. As noted above plain-carbon steels are subject to cracking when quenched too quickly. More likely, this is an alloy steel where fine pearlitic microstructures can be developed because alloying elements inhibit the austenite \rightarrow ferrite + pearlite transformation. The microstructure in Figures 7a and b is consistent with an alloy steel that has been normalized and air cooled.

Figure 8 a, b, c, and d are from an Exxon coupling box field return. The microstructure is often referred to as "banded" ferrite (light) and pearlite (dark). In this case, the banding originates from the extrusion process used to form the rod stock. This microstructure is consistent with a fully annealed alloy steel which would be the condition of an extruded steel without any further thermal processing.

Characterization of Failed Field Returns

Visual examination showed that failed pins and coupling boxes were fatigue-type failures characterized by several common features. In all of the pin field returns, failure initiated in the first thread fully engaged in the box (the thread closest to the shoulder of the sucker rod). No failures were observed in the shoulder region. The fracture surface contained a smooth fatigue crack growth region that was perpendicular to the load axis. The smoothness is attributed to the crack walls rubbing against one another during repetitive loading and unloading. The fatigue crack region was estimated to cover between 30 and 70% of the cross sectional area of the pin. The remaining area showed a morphology consistent with ductile overload failure. Corrosion product, predominantly rust that appeared to associated with the crack, was observed at or near all of the fracture surfaces. The extent to which the environment may have

embrittled the steel or accelerated cracking could not be determined since the fatigue region of the fracture surface was rubbed smooth by mechanical action.

Visual examination showed that box failures also exhibited common features. Box fracture surfaces exhibited two regions. The first was a smooth fatigue region whose surface was oriented perpendicular to the load axis. The second was a ductile rupture region similar to that observed in the failed pins. There were sufficient beach mark remnants on these fatigue regions to indicate that cracks grew from inside out in each case. Cracks appeared to originate in the last fully engaged pin thread in the box in each of the failed field returns.

Metallographic examination showed that sub-critical cracks (cracks that did not result in fracture) were observed in several specimens. Figure 9a, b, and c are optical micrographs of a crack that initiated at the base of a thread in the middle of the threaded region of a pin. This particular pin failed at the top—most fully engaged thread. Cracks that initiate at the base of threads are expected since thread roots are stress concentrators. This crack probably initiated after the crack that led to failure.

Figure 10 shows a crack that initiated midway between the thread root and the thread tip. In a properly made up pin-box joint, cracking in this location is not expected. However, if there is loosening of the joint, known as "loss of displacement", or if the joint is improperly made, the thread tips of the pin may be subject to a shear load that could initiate cracks like the one shown in Figure 10.

Overview of Fatigue Properties of Plain-Carbon and Alloy Steels

With respect to fatigue life, metals tend to fall in two groups. Either the metal or alloy exhibits a well defined fatigue limit (defined as a stress amplitude) below which the material is essentially immune from cyclic damage, or there is no stress limit below which the metal is immune from cyclic damage. Ferrous alloys typically exhibit a fatigue limit when tested in air, but do not exhibit a fatigue limit under corroding conditions¹³. The corrosive conditions down hole are likely to have accelerated fatigue type failures although the extent to which corrosion contributes to this process is not well known.

Corrosion effects aside, the fatigue properties of plain-carbon and alloy steels are well known and there are several rules of thumb used in fatigue design and alloy selection that are pertinent to sucker rod strings^{14,15}. Normally, the fatigue limit is taken to be one-half the ultimate tensile strength (UTS). This relationship is quite good for steels with UTS values up to 150 ksi which includes all steels encompassed by the API specification. It should be noted however, that the ratio of fatigue strength to UTS does vary between about 0.35 and 0.60 for several alloy and plain-carbon steels as shown in Figure 11¹⁵ and that sensitivity to the presence of notches increases with increasing tensile strength. Since fatigue strength is closely related to tensile strength, it follows that alloy chemistry, thermomechanical treatment and ferrite/pearlite distributions will affect fatigue behavior^{16,17,18}.

Experimental evidence indicates that homogenizing or dispersing slip, so that local concentrations of plastic deformation do not arise, is an effective way to improve fatigue properties¹⁹. For example, a much lower fatigue limit is observed in a pearlite steel with a coarse microstructure than in a spheroidite steel with a fine microstructure even though the two had the same compositions and tensile strengths²⁰. The coarse ferrite-pearlite structure of the sucker rod pin shown in Figure 6a and b might be expected to have a lower fatigue limit than that of the fine microstructure of Figures 7a and b for the same reasons. For heat treatable alloy steels, quenched and tempered microstructures are considered optimum for smooth bar fatigue resistance^{14,21}.

Although large non-metallic inclusions do not significantly affect tensile strength, they can act as fatigue crack nuclei causing a reduced performance under cyclic loading^{22,23}. Advances in steel making, particularly degassing and vacuum melting, can reduce exogenous

inclusion contents to produce steels with improved fatigue performance¹⁴. As a general rule, the sensitivity of fatigue properties to inclusions increases with increasing tensile strength.

Since the majority of sucker rod pins and box coupling failures are associated with machined threads⁵, the effects of notches (e.g., the thread roots) and residual surface stresses (due to machining) are important. Under axial loading of the sucker rod and box coupling, tensile stresses are concentrated at thread roots. The effect of notches like thread roots on fatigue life has been determined experimentally by comparing S-N (stress amplitude vs. cycles) data obtained from notched and unnotched specimens, and theoretically by modeling and calculation. These data are usually reported as notch sensitivity and stress concentration factors²⁴. Usually, notch sensitivity increases with tensile strength. As a result, higher tensile strength materials may exhibit lower than expected fatigue performance when notches are present as shown in Figure 12 for quenched and tempered steels and normalized steels.

Surface residual stresses can impact fatigue performance since fatigue cracks almost always initiate at surfaces. Compressive stresses due to machining, shot peening, carburization, or induction hardening have a beneficial effect on inhibiting fatigue crack initiation²⁵ and growth²⁶. This is why machined threads are preferred over forged threads on sucker rod pins. Surface hardening by rapid quenching is sometimes used in the automotive industry to improve fatigue performance^{27,28}. Residual tensile stresses at the surface do tend to accelerate fatigue crack growth, but the effect is, in some instances, reported to be small²⁶.

To summarize, fatigue strength does increase with yield strength, although this increase is not always proportional. A convenient rule of thumb is that the fatigue strength is approximately one-half of the tensile strength. As a result, the use of many high strength materials is fatigue limited. Fatigue properties are highly structure sensitive whereas tensile properties are less so. This raises some concerns since sucker rod pin and coupling failures are almost always due to fatigue, but the API sucker rod specification delineates rod grade by composition and tensile strength, instead of by fatigue life and microstructure. Some gains in fatigue life can be made through microstructural control by thermomechanical processing, although it is generally believed that intelligent design and alloy selection are more effective ways to combat fatigue.

Summary

The major elements examined in this paper are failure data collection, finite element analysis of the threaded connection, and metallographic and fatigue analysis. As mentioned in the paper, there are many other factors that impact the failure of a sucker rod/sinkerbar string that are not studied here.

Failure data collection is a key to understanding and eventually minimizing rod string failures. Only through knowledge of where failures occur in the string, what stress and corrosive environment existed before failure, and the dynamics of the pumping string, will it be known what caused the failure. Knowing why a failure occurs is the first step to preventing it from occurring again. In addition, data collection illustrates the magnitude of the problem, which is instrumental to mobilizing the personnel and resources to minimize the problem in the future.

Finite element analysis of the threaded connection is an inexpensive and quick method to quantify the performance of the connection under a wide variety of loading conditions. While the current analysis is limited primarily to demonstrating a capability, it does show a possible correlation with the metallographic analysis in the location of micro-fractures on the thread faces. This analysis also shows the distribution of stresses in the relatively simple loading step of merely threading the connection together to achieve a desired prestress. Maximum tensile

and compressive stresses locate places that need further study and are candidate locations for modification under new designs.

Fatigue and corrosion fatigue failures constitute a significant fraction of sucker rod pin and coupling failures. A review of pertinent fatigue literature for plain-carbon and alloy steels, and a microstructural characterization of pin and couplings from the field were performed to determine if any significant benefit could be expected by controlling the processing and microstructure of the steels used to fabricate sucker rods. The API specification for steels that may be furnished for sucker rods is quite broad and encompasses most plain-carbon and alloy steels. A broad range of ferrite-pearlite microstructures were observed in metallographic examination of field returns. Fatigue literature shows for sucker rod steels, the rule of thumb that the fatigue strength is roughly equal to one-half the tensile strength, is valid. It must be recognized, however, that fatigue properties are much more structure sensitive than tensile properties. The effects of exogenous inclusions, notches, and ferrite/pearlite proportions and distribution can have a large impact on fatigue life. Selection of a steel based on tensile properties, without regard for microstructure for service dominated by cyclic loading may not always be appropriate. Although some gains in fatigue life might be made through microstructural control, it is more likely that intelligent design and alloy selection are more effective ways to combat fatigue failure.

References

- 1) R. Rothrock, Jr.: "Downhole Maintenance Costs Approach \$2 Billion," **The Petroleum Engineer**, July, 1977.
- 2) **Oil & Gas Journal**: "Worldwide Production Report," December 10, 1991.
- 3) Sandia National Laboratories Sucker Rod/Sinker Bar Pin Study Group Meeting, January 31, 1992.
- 4) K.H. Moore, **Petroleum Engineer Int.**, reprint from July, 1981, p. H-1.
- 5) Amoco, Midland Farms Service Data presented at Sandia Sucker Rod/Sinker Bar Study Group Meeting, January 31, 1992.
- 6) K. Nudge, C.J. Levesque, **Oil and Gas Journal**, Sept., 27, 1982, p. 245.
- 7) **Corrosion of Oil and Gas Well Equipment**, NACE and API, Dallas TX, 1958.
- 8) Flexbar, Inc. Product Literature, Flexbar Inc., Odessa, TX, 1992.
- 9) Specification for Sucker Rods (Pony Rods, Polished Rods, Couplings and Subcouplings), API Specification 11B, 24th Ed., Cot., 1, 1990, API, Dallas, TX.
- 10) T.D. Blacker: "FASTQ Users Manual Version 1.2," **SAND88-1326**, Sandia National Laboratories, Albuquerque, NM, June, 1988.
- 11) **ABAQUS User's Manual Version 4.8**, Hibbitt, Karlsson, and Sorensen, Inc., 1989.
- 12) Supplied by A. Pena, Exxon Production Operations, Southwestern Division.

- 13) H.W. Boyer, ed., **Atlas of Stress Strain Curves**, ASM International, Materials Park, OH, 1987.
- 14) C.C. Osgood, **Fatigue Design**, 2nd ed., Pergamon Press, New York, 1982, p. 467-477.
- 15) R.W. Hertzberg, **Deformation and Fracture Mechanics**, 2nd ed., John Wiley & Sons, Inc., New York, p. 457-511.
- 16) D.M. Jankowski, Conference Proceedings:**Fatigue Life Analysis and Prediction**, V.S. Goel, Ed., American Society for Metals, Metals Park, OH, 1986, p. 203.
- 17) S.K. Sasaki, Y. Ochi, A. Ishii, H. Abe, **JSME International Journal**, Series I, vol. 33, no. 2, 1990, p. 155.
- 18) M. Goto, Y. Yanagawa, H. Nisitani, **JSME International Journal**, Series I, vol. 33, no. 2, 1990, p. 235.
- 19) J.C. Grosskreutz, **Metall. Trans.**, vol. 3., 1972, p. 1255.
- 20) G.E. Dieter, R.F. Mehl, G.T. Horne, **Trans. Am. Soc. Met.**, vol. 47, 1953, p. 423.
- 21) **Fatigue Design Handbook**, AE-10, Society of Automotive Engineers, R.C. Rice, ed., SAE, Inc., Warrendale, PA, 1988.
- 22) T.A. Khalfia, **J. Mat. Sci. Lett.**, no. 8, 1988, p. 427.
- 23) Y. Murakami, S. Kodama, S. Konuma, **Int. J. Fatigue**, vol. 11, no. 5, 1989, p. 291.
- 24) G.E. Dieter, **Mechanical Metallurgy**, McGraw-Hill, New York, 1986, p. 402.
- 25) R.W. Landgraf, R.A. Chernenkoff, "Residual Stress Effects of Surface Processed Steels", **Analytical and Experimental Methods for Residual Stress Effects in Fatigue**, ASTM STP 1004, R.L. Champoux, Ed., ASTM, Philadelphia, PA, 1988, p. 1-12.
- 26) A. Okamoto, H. Nakamura, **J. Pressure Vessel Tech.**, 112, Aug., 1990, p. 199.
- 27) R.F. Kern, **Heat Treating**, Sept., 1986, p. 19.
- 28) M. Imagumbi, K. Nishioka, Y. Terada, Conference Proceedings: **Microstructure and Mechanical Behavior of Materials**, vol. 2, EMAS, Warley, UK, 1986, p. 885.

Acknowledgement

The work presented in this report represents a response to industry under the US Department of Energy's Oil Recovery Technology Partnership. The authors wish to acknowledge the insights provided by all the industry personnel whom we have interacted with during the course of this project.

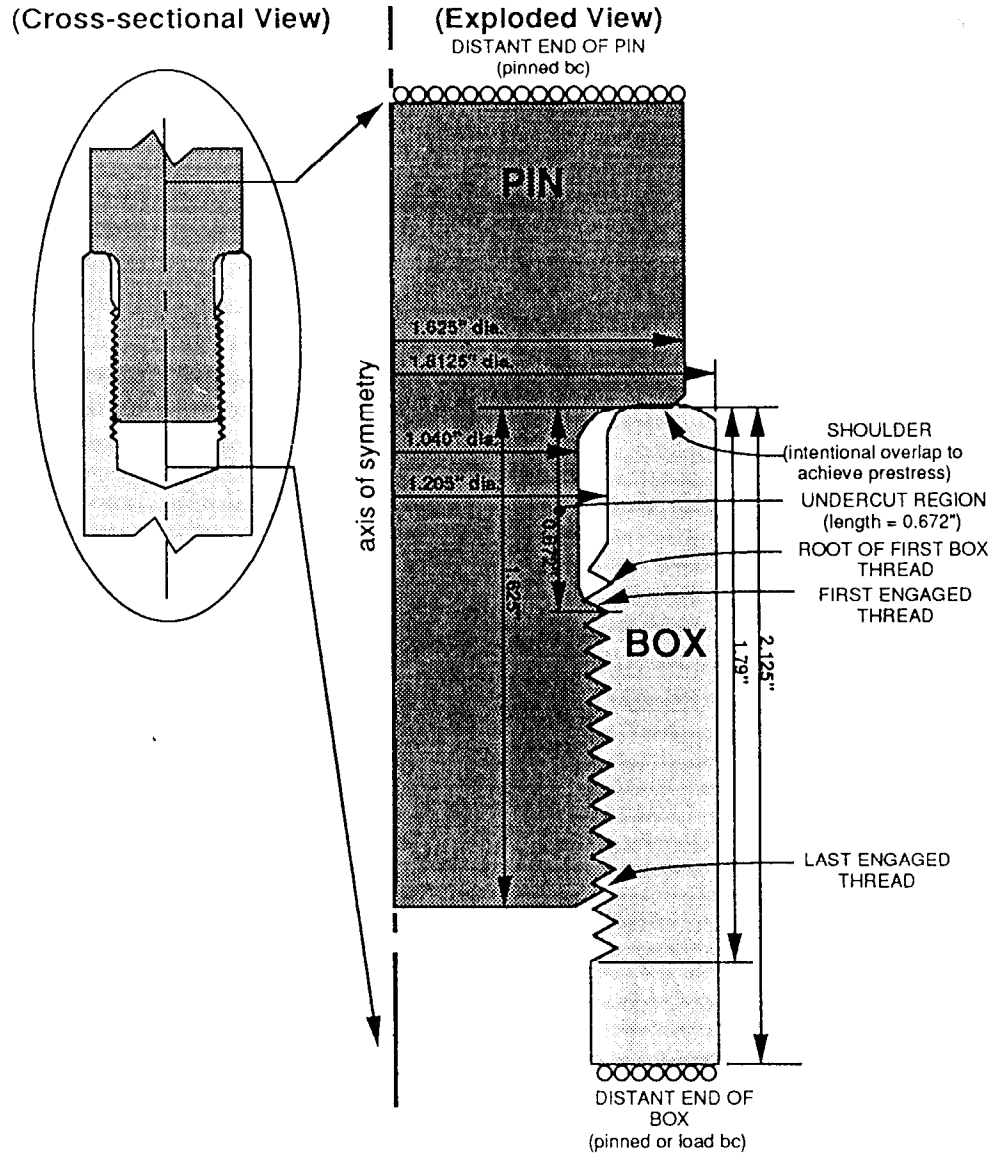


Figure 1 - 7/8" API box and pin sucker rod connection with dimensions and terminology

7/8" API Box and Pin Sucker Rod Connection

(Thread Detail)

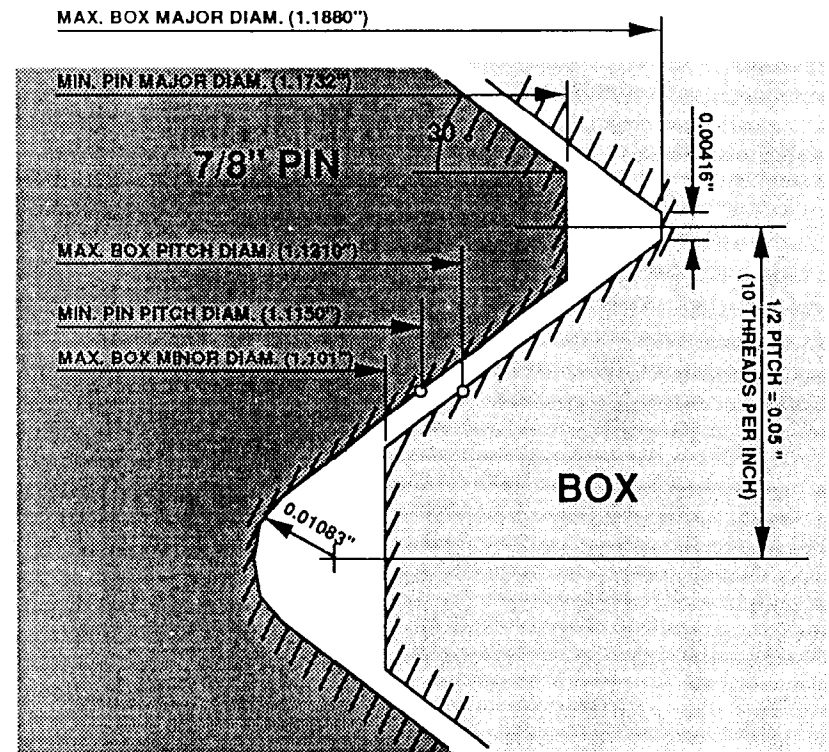


Figure 2 - 7/8" API sucker rod box and pin thread form

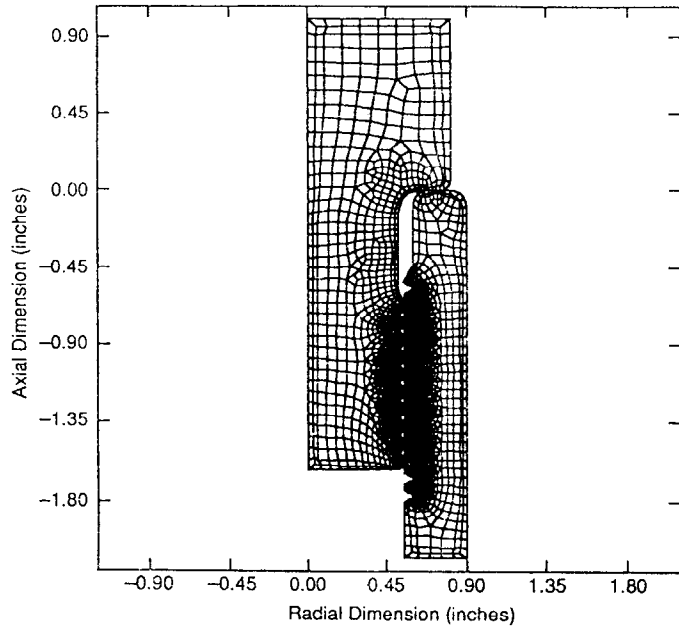


Figure 3a - Undeformed mesh plot of sucker rod connection simulated - full view

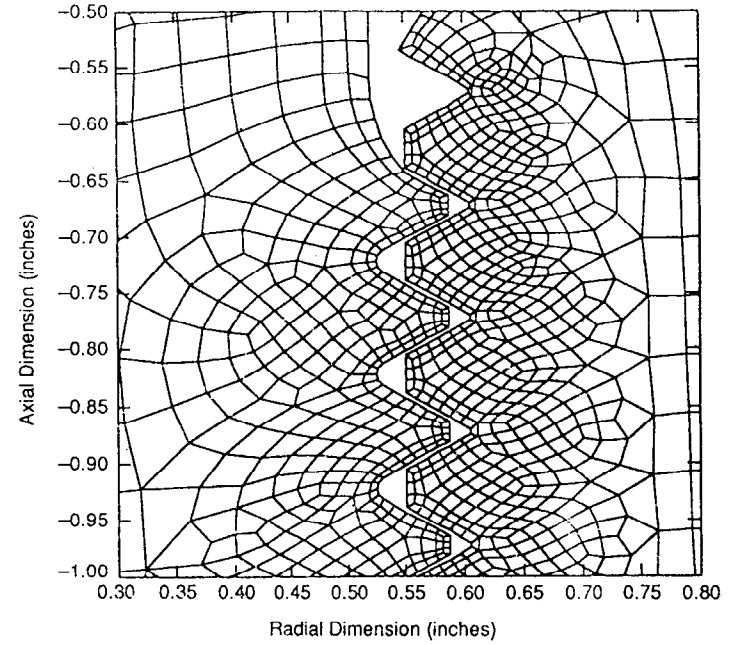


Figure 3b - Undeformed mesh plot of sucker rod connection simulated - 4 thread view

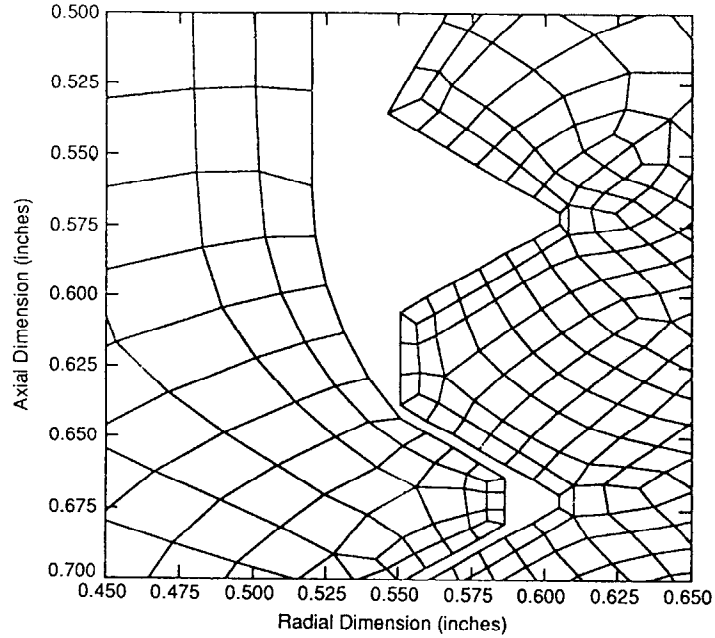


Figure 3c - Undeformed mesh plot of sucker rod connection simulated - first thread view

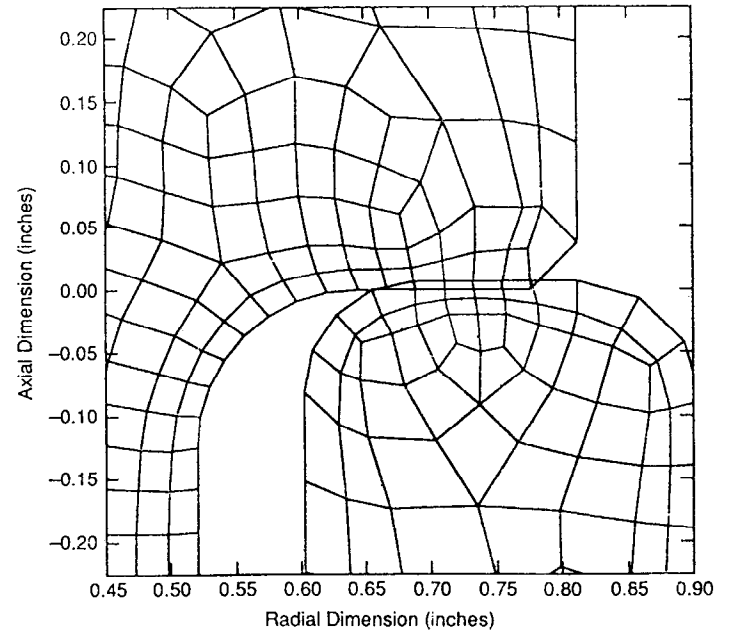
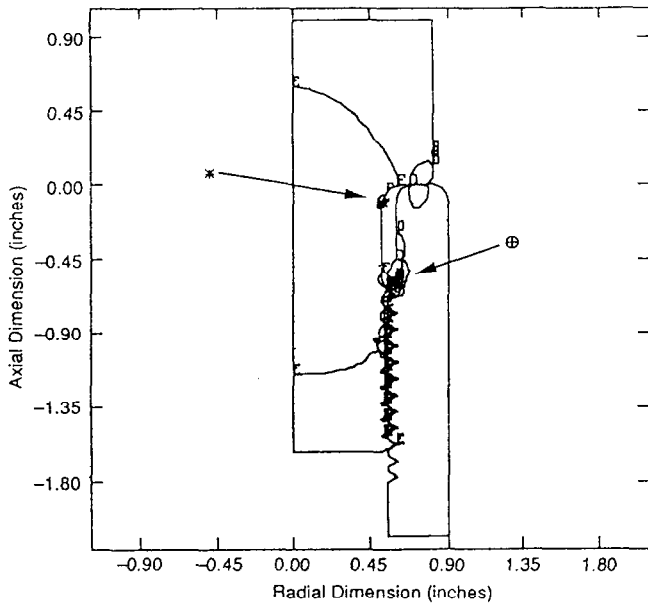


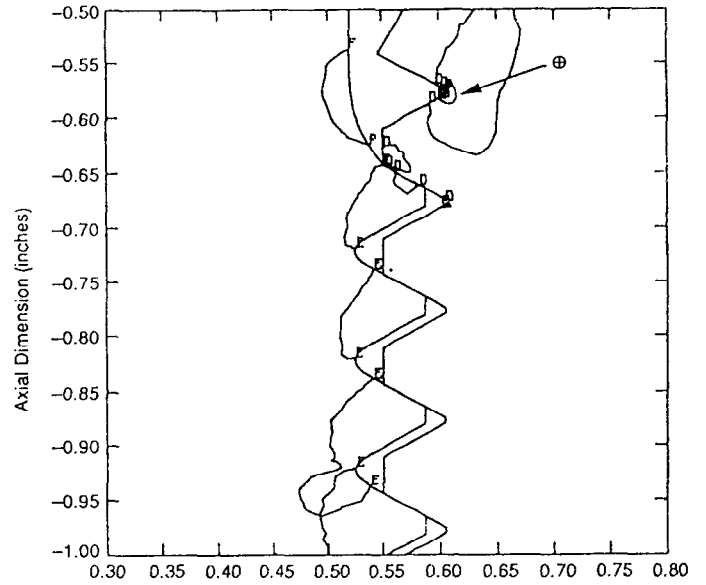
Figure 3d - Undeformed mesh plot of sucker rod connection simulated - shoulder view



Axial Stress
(+ Tension, - Compression)

- A = -75000. PSI
- B = -55000. PSI
- C = -35000. PSI
- D = 5000. PSI
- E = 25000. PSI

- ⊕ = -62480. PSI (Max. compression)
- * = 31290. PSI (Max. tension)



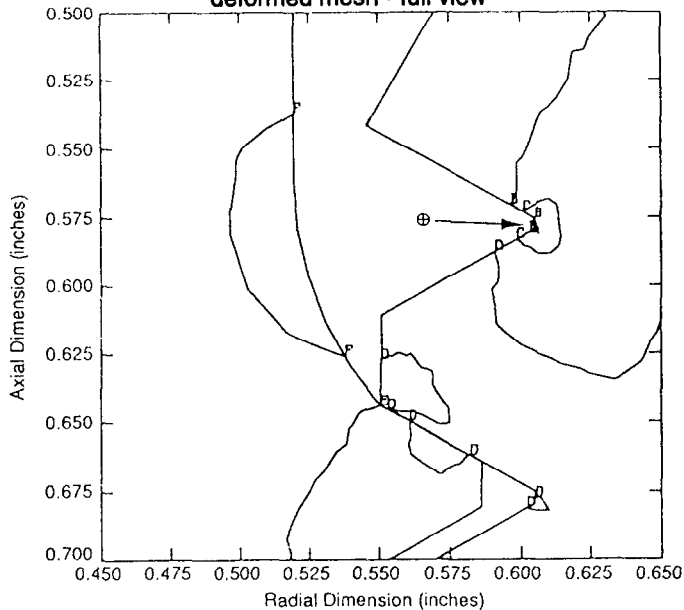
Axial Stress
(+ Tension, - Compression)

- A = -75000. PSI
- B = -55000. PSI
- C = -35000. PSI
- D = 5000. PSI
- E = 25000. PSI

- ⊕ = -62480. PSI (Max. compression)
- * = 31290. PSI (Max. tension)

Figure 4a - Axial stress component contour on deformed mesh - full view

Figure 4b - Axial stress component contour on deformed mesh - 4 thread view

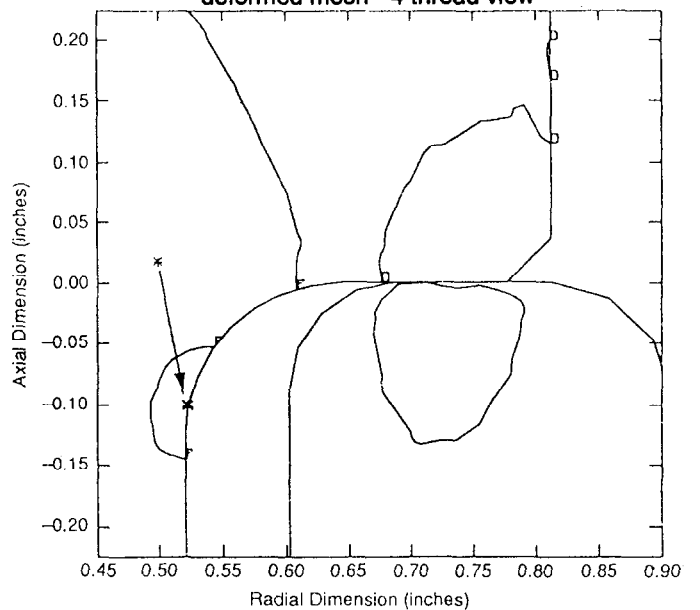


Axial Stress
(+ Tension, - Compression)

- A = -75000. PSI
- B = -55000. PSI
- C = -35000. PSI
- D = 5000. PSI
- E = 25000. PSI

- ⊕ = -62480. PSI (Max. compression)
- * = 31290. PSI (Max. tension)

Figure 4c - Axial stress component contour on deformed mesh - first thread view

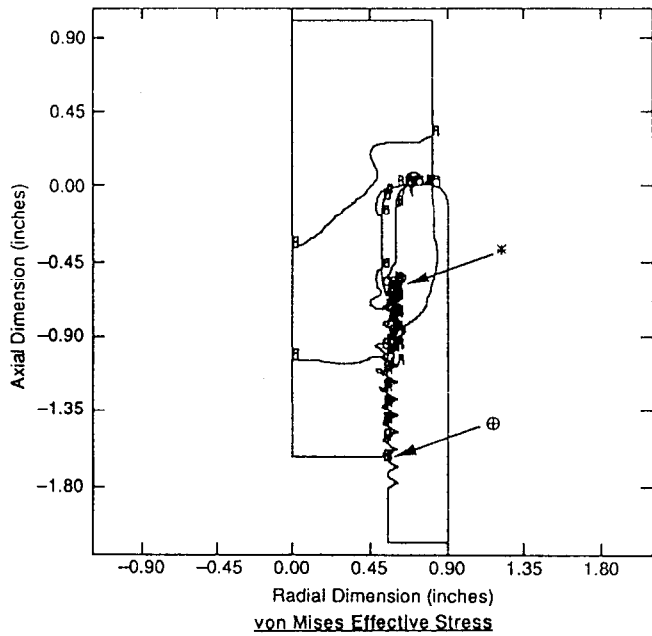


Axial Stress
(+ Tension, - Compression)

- A = -75000. PSI
- B = -55000. PSI
- C = -35000. PSI
- D = 5000. PSI
- E = 25000. PSI

- ⊕ = -62480. PSI (Max. compression)
- * = 31290. PSI (Max. tension)

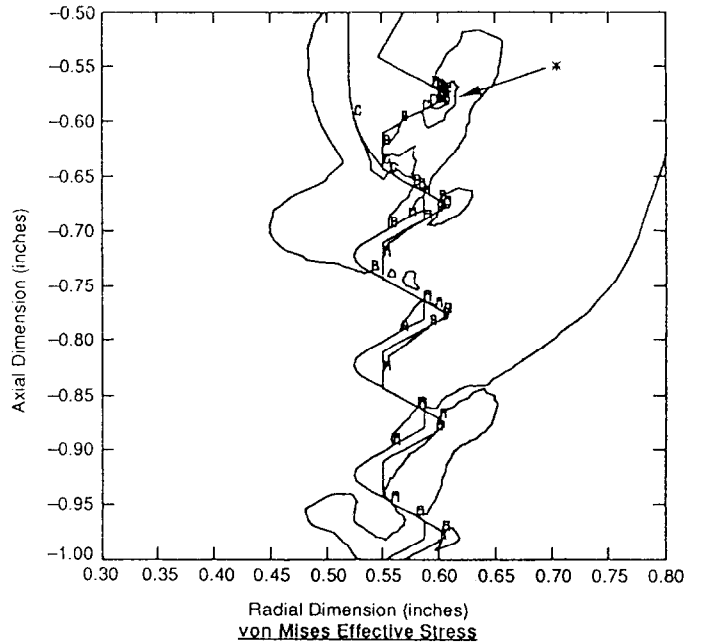
Figure 4d - Axial stress component contour on deformed mesh - shoulder view



A = 10000. PSI
 B = 20000. PSI
 C = 30000. PSI
 D = 40000. PSI
 E = 50000. PSI
 F = 60000. PSI

 ⊕ = 80. PSI (Minimum)
 * = 63570. PSI (Maximum)

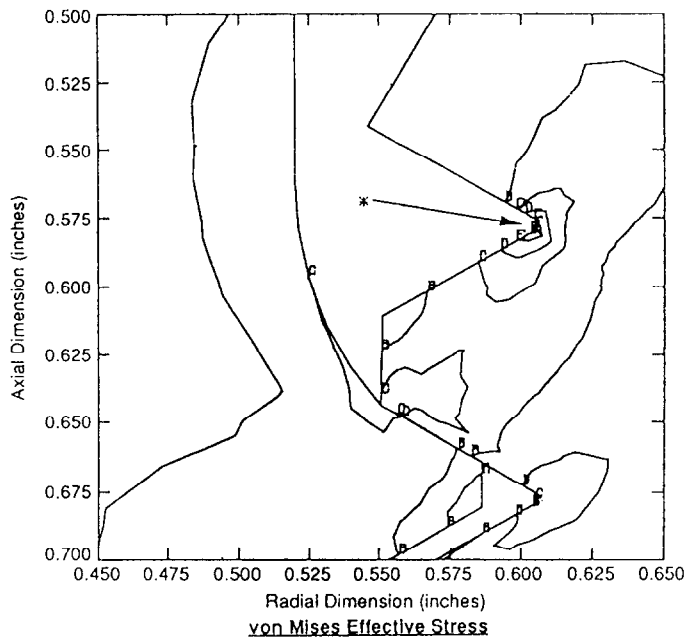
Figure 5a - von Mises effective stress contour on deformed mesh - full view



A = 10000. PSI
 B = 20000. PSI
 C = 30000. PSI
 D = 40000. PSI
 E = 50000. PSI
 F = 60000. PSI

 ⊕ = 80. PSI (Minimum)
 * = 63570. PSI (Maximum)

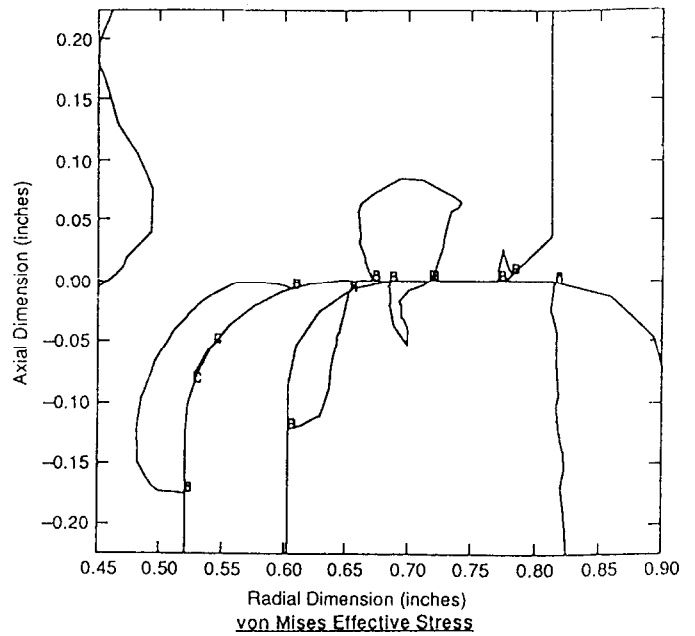
Figure 5b - von Mises effective stress contour on deformed mesh - 4 thread view



A = 10000. PSI
 B = 20000. PSI
 C = 30000. PSI
 D = 40000. PSI
 E = 50000. PSI
 F = 60000. PSI

 ⊕ = 80. PSI (Minimum)
 * = 63570. PSI (Maximum)

Figure 5c - von Mises effective stress contour on deformed mesh - first thread view



A = 10000. PSI
 B = 20000. PSI
 C = 30000. PSI
 D = 40000. PSI
 E = 50000. PSI
 F = 60000. PSI

 ⊕ = 80. PSI (Minimum)
 * = 63570. PSI (Maximum)

Figure 5d - von Mises effective stress contour on deformed mesh - shoulder view

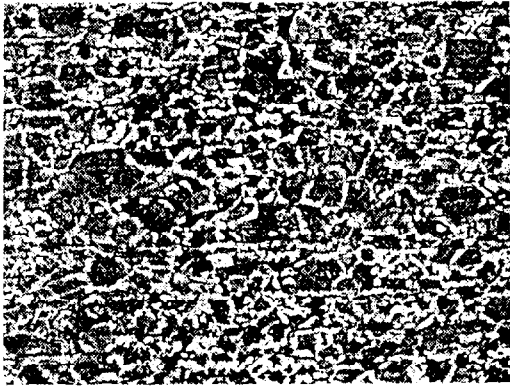


Figure 6a - Optical micrograph of Flexbar's lower grade sucker rod (100x)



Figure 6b - Optical micrograph of Flexbar's lower grade sucker rod (500x)

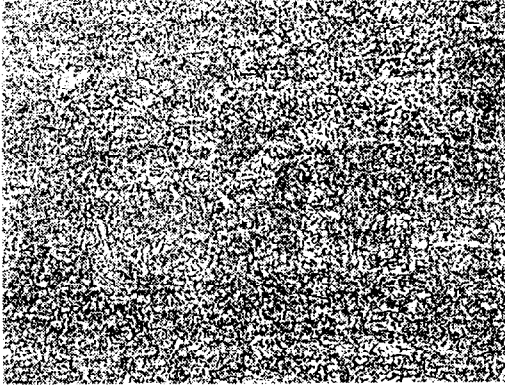


Figure 7a - Optical micrograph of Flexbar's higher grade sucker rod (100x)

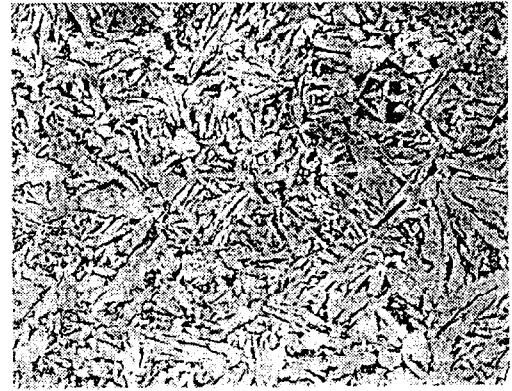


Figure 7b - Optical micrograph of Flexbar's higher grade sucker rod (500x)

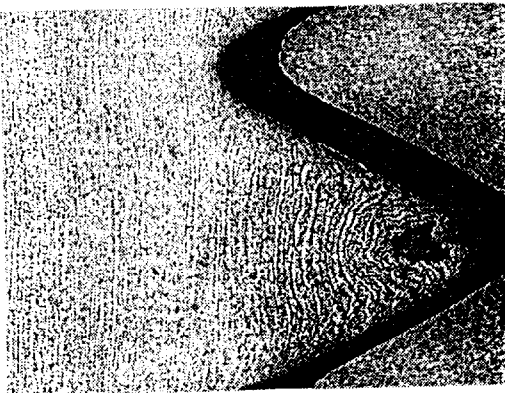


Figure 8a - Exxon field return (32x)

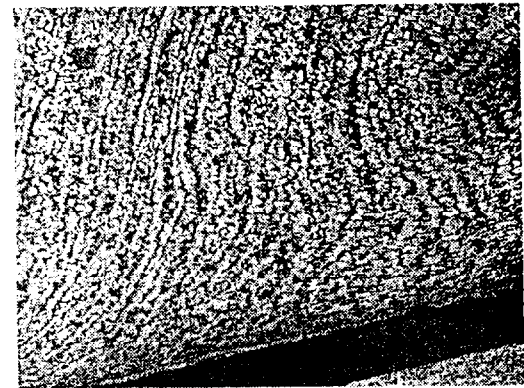


Figure 8b - Exxon field return (100x)

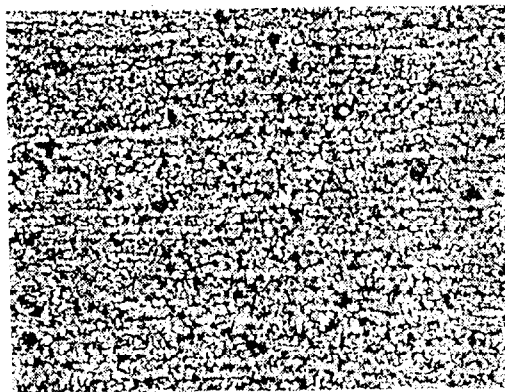


Figure 8c - Exxon field return (100x)

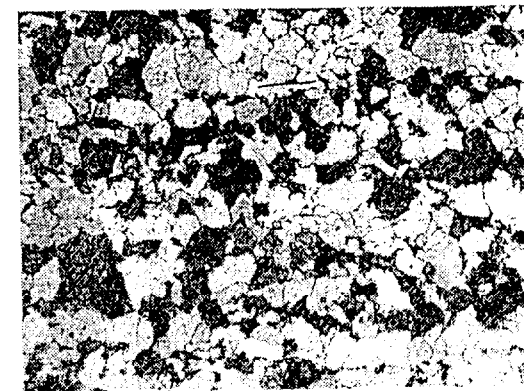


Figure 8d - Exxon field return (500x)

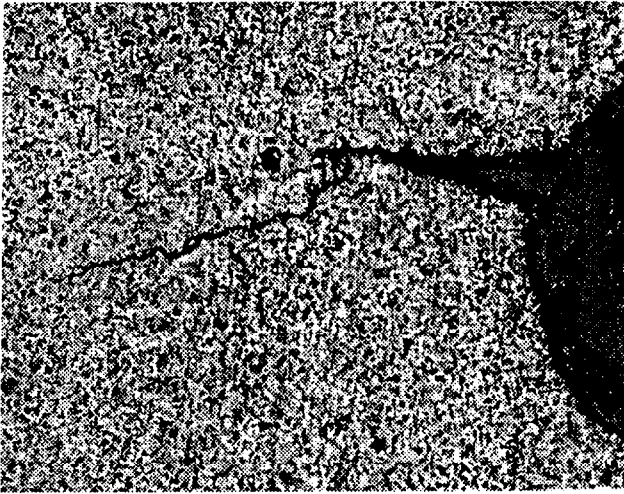


Figure 9a - Exxon field return (50x). Sub-critical fracture in root of pin thread.

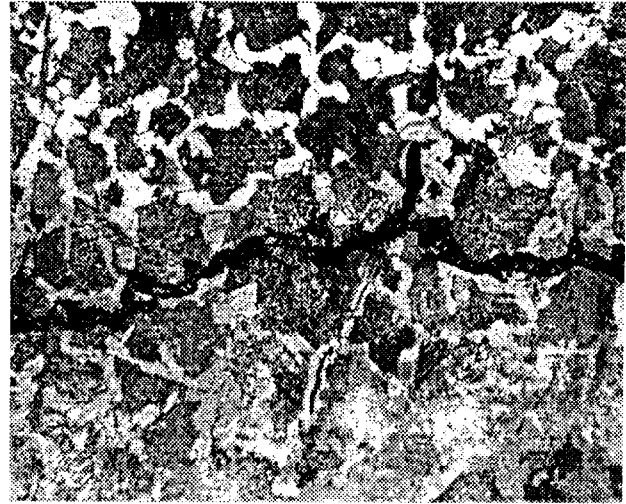


Figure 9b - Exxon field return (500x). Same fracture as in Figure 9a.

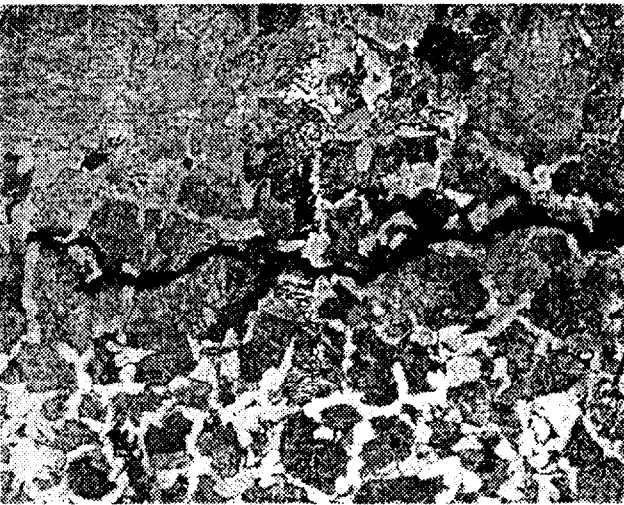


Figure 9c - Exxon field return (500x). Same fracture as in Figures 9a,b.

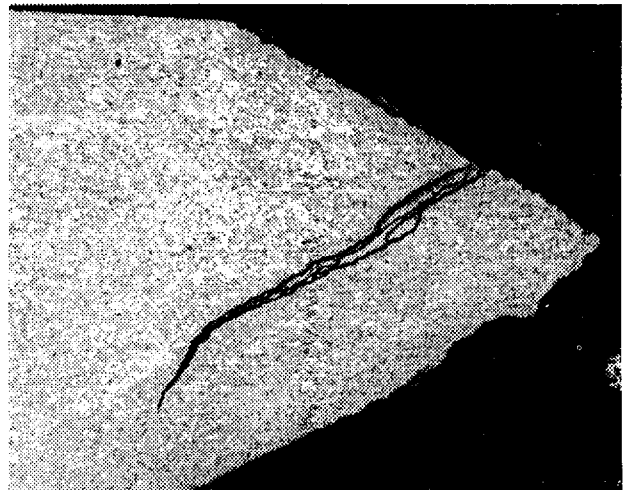


Figure 10 - Exxon field return (50x). Sub-critical fracture in pin thread.

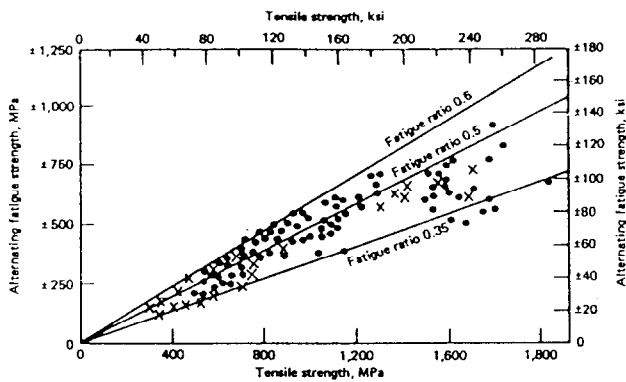


Figure 11 - Relationship between rotating, bending unnotched fatigue strength and tensile strength for alloy (+) and plain-carbon (x) steels. After (15).

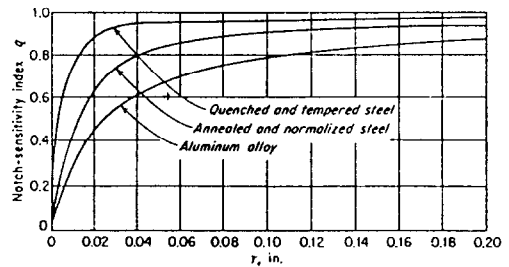


Figure 12 - Variation of notch sensitivity index with notch radius for materials with different tensile strengths.